JOURNAL OF THE ROYAL SOCIETY Interface

J. R. Soc. Interface (2008) **5**, 339–348
doi:10.1098/rsif.2007.1077
Published online 13 June 2007

Frictional and elastic energy in gecko adhesive detachment

Nick Gravish, Matt Wilkinson and Kellar Autumn*

Department of Biology, Lewis and Clark College, Portland, OR 97219, USA

Geckos use millions of adhesive setae on their toes to climb vertical surfaces at speeds of over $1\ \mathrm{m\ s^{-1}}$. Climbing presents a significant challenge for an adhesive since it requires both strong attachment and easy, rapid removal. Conventional pressure-sensitive adhesives are either strong and difficult to remove (e.g. duct tape) or weak and easy to remove (e.g. sticky notes). We discovered that the energy required to detach adhering tokay gecko setae (W_{d}) is modulated by the angle (θ) of a linear path of detachment. Gecko setae resist detachment when dragged towards the animal during detachment ($\theta = 30°$) requiring $W_{\mathrm{d}} = 5.0 \pm 0.86$ (s.e.) $\mathrm{J\ m^{-2}}$ to detach, largely due to frictional losses. This external frictional loss is analogous to viscous internal frictional losses during detachment of pressure-sensitive adhesives. We found that, remarkably, setae possess a built-in release mechanism. Setae acted as springs when loaded in tension during attachment and returned elastic energy when detached along the optimal path ($\theta = 130°$), resulting in $W_{\mathrm{d}} = -0.8 \pm 0.12\ \mathrm{J\ m^{-2}}$. The release of elastic energy from the setal shaft probably causes spontaneous release, suggesting that curved shafts may enable easy detachment in natural, and synthetic, gecko adhesives.

Keywords: gecko; adhesion; energy; friction; biomechanics; tribology

1. INTRODUCTION

Geckos' climbing ability is nearly unrivalled in nature. Geckos are able to climb microscopically smooth surfaces as fast as other terrestrial animals can run on level ground (Autumn *et al.* 2006*b*). Key to geckos' amazing feats are millions of adhesive setae segmented into scansors on the undersides of the toes. Gecko setae form a smart (Fakley 2001) fibrillar adhesive that is capable of strong attachment and rapid and easy detachment. The work of detachment (W_{d}; the integral of the forces along the detachment path during unloading) represents an adhesive's ability to resist failure (Zosel 1985). Highly tenacious pressure-sensitive adhesives (PSAs) such as duct tape are capable of absorbing large detachment energies (W_{d}) yet also require a similarly large W_{d} for removal. Ideally, a smart adhesive would be capable of absorbing large detachment energies (W_{d}) while attached, but require only a small W_{d} during removal. This study focuses on the apparently contradictory design principles underlying adhesion and removal of gecko setae.

1.1. Conventional pressure-sensitive adhesives

Comparisons between the gecko adhesive and conventional PSAs yield striking similarities and profound differences (Autumn 2006*b*). Both PSAs and geckos adhere primarily by van der Waals (vdW) forces (Autumn *et al.* 2002; Creton 2003) and have effective elastic moduli below 100 kPa (Dahlquist 1969; Pocius 2002; Autumn *et al.* 2006*c*), but gecko setae stand in stark contrast to PSAs in their anisotropy (Autumn *et al.* 2006*a*) and self-cleaning (Hansen & Autumn 2005) properties. PSAs are used commonly for both industrial and home applications. Post-It notes contain a PSA that detaches easily from most surfaces, whereas double-sided tape is used typically for structural applications requiring strong permanent attachment (Creton 2003). However, a single conventional PSA cannot adhere strongly and also detach easily. Yet, the normal operation of the gecko adhesive demands both strong attachment and rapid detachment.

The thermodynamic work of adhesion (γ) for vdW interactions is approximately $50\ \mathrm{m\ J\ m^{-2}}$ (Israelachvili 1992) yet W_{d} is typically orders of magnitude larger in PSAs (Kinloch 1987; Creton & Fabre 2002) as a result of viscoelastic energy loss occurring from internal friction processes such as cavitation and fibrillation of the adhesive (Creton & Fabre 2002) that lead to material degradation. Gecko setae must maintain their structure and adhesive capability over the course of the animal's moult cycle, approximately two months (K.A. & N.G. 2006, personal observation). The viscous deformation typical of detaching PSAs does not seem to occur in the gecko adhesive, which deforms elastically, not plastically (Autumn *et al.* 2006*c*). This suggests that if W_{d} is indeed large in gecko setae, viscous deformation may not be the primary mechanism of energy loss.

*Author for correspondence (autumn@lclark.edu).

Electronic supplementary material is available at http://dx.doi.org/10.1098/rsif.2007.1077 or via http://journals.royalsociety.org.

Received 13 April 2007
Accepted 24 May 2007

1.2. Do fibrillar adhesives yield large W_d?

Measurements of W_d in soft rubbers illustrate that highly elastic systems are capable of dissipating energy upon detachment ($W_d \gg \gamma$; Lake & Thomas 1967). The long-chain polymers that make up soft rubbers are cross-linked at large intervals, thereby eliminating local elastic energy return that would otherwise occur during polymer bond rupture and thus results in large W_d (Lake & Thomas 1967). Jagota & Bennison (2002) noted that the gecko adhesive similarly lacks material cross links and proposed that setal fibrils may dissipate elastic energy, resulting in large W_d (Jagota & Bennison 2002). However, the comparison between rubber polymer chains and gecko setae can only be extended so far, as the elastic energy dissipation mechanism in rubbers limits the minimum energy dissipation that occurs, not the maximum (Lake & Thomas 1967). In soft rubbers, large energy dissipation ($W_d \gg \gamma$) will occur regardless of the detachment method. Thus, this elastic dissipation mechanism would not seem to satisfy the gecko's smart adhesion requirements by enabling strong attachment, yet hindering efficient detachment. To investigate fully the smart adhesive properties of gecko setae, we must consider their unique anisotropy.

1.3. Anisotropic geometry and function of the tokay gecko adhesive

Tokay gecko (*Gekko gecko*) setae are approximately 110 μm in length, 4.2 μm in diameter, and branch at the tips into hundreds of 200 nm wide spatular pads (figure 1; Ruibal & Ernst 1965; Russell 1975; Williams & Peterson 1982; Autumn *et al.* 2006*c*). Setae are curved and oriented at approximately 45°, pointing distally (away from the animal), which produces anisotropic shear and normal forces (Ruibal & Ernst 1965; Russell 1975; Williams & Peterson 1982; Autumn *et al.* 2006*c*; Tian *et al.* 2006).

The geometry and function of the tokay gecko seta suggest that to investigate the adhesive's detachment mechanics, both friction and adhesion effects must be considered. Setal attachment requires a perpendicular preload followed by a small proximal drag (towards the animal) that loads seta tensily (Autumn *et al.* 2000). Once setae engage, a proximally oriented shear force maintains setal tension and produces adhesion, possibly by elongating the peel zone of the spatula (Tian *et al.* 2006). A distally directed shear force releases tension and results in no adhesion. Whole animal adhesion measurements show that the tokay gecko's adhesive detaches when the applied detachment force increases above an angle, $\alpha = 26$–$30°$ (Autumn *et al.* 2006*a*) relative to the substrate. This maximum detachment force angle (α^*) coincides directly with the maximum setal–substrate shaft angle at which point setae spontaneously detach (Autumn *et al.* 2006*a*). Increasing the setal shaft angle or applied detachment force angle above $\alpha = 26$–$30°$ probably causes fracture of the spatula–substrate bonds (Autumn *et al.* 2000) and thus detachment. However, it is not known how adhering gecko setae respond to applied displacements at varied detachment path angles (θ).

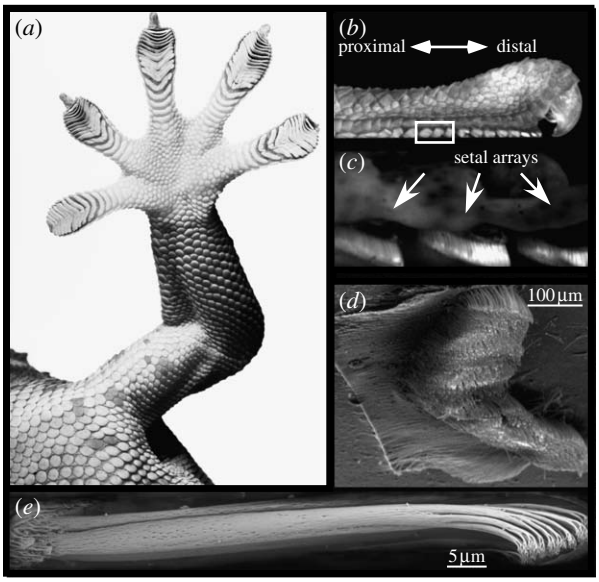

Figure 1. An overview of the gecko adhesive from macroscale to microscale. (*a*) A tokay gecko's toes are covered in adhesive hairs (setae). (*b*) Setae are grouped into arrays along the underside of the toe. Pulling setal arrays in the proximal direction produces adhesion and high friction. Pushing distally causes no adhesion to occur and low friction. (*c*) Setal arrays along the underside of the toe. (*d*) Setal arrays are densely packed but achieve high contact areas owing to setal branching and flexibility. (*e*) A single seta is approximately 110 μm in length and 2.1 μm in radius. Setae have a slight curvature and branch at their tips ending in 200 nm wide spatula.

Climbing geckos stay attached to surfaces because they pull their limbs proximally (towards the animal) during the stance phase of the stride (Autumn *et al.* 2006*b*). Proximal shearing of the adhesive generates friction and adhesion maintaining attachment (Autumn *et al.* 2006*a*). At the initiation of the swing phase of the stride, geckos relax shear force, detaching the adhesive rapidly in approximately 15 ms with no measured reactant forces (Autumn *et al.* 2006*a*,*b*). The climbing dynamics of the gecko demonstrate the directional (proximal–distal) force control of the gecko adhesive's stickiness. Strong attachment of the adhesive results from proximal shearing as the gecko pulls inward towards the centre of mass (Autumn *et al.* 2006*a*,*b*). Detachment of the foot probably occurs along a vertical ($\theta = 90°$) or distal ($\theta > 90°$) path, but this remains unknown. Here, we present the first experimental measurement of the amount of energy (W_d) required to detach isolated gecko setae over a linear detachment path of angle θ. W_d measured while detaching in the proximal direction ($\theta < 90°$) represents the adhesive's ability to resist failure while trying to maintain attachment. W_d measured during distal detachment ($\theta > 90°$) represents the ease of detachment.

2. MATERIAL AND METHODS

We harvested and mounted 17 setal arrays from five live non-moulting tokay geckos (*G. gecko*) using the methods modified from Autumn *et al.* (2002). Under a

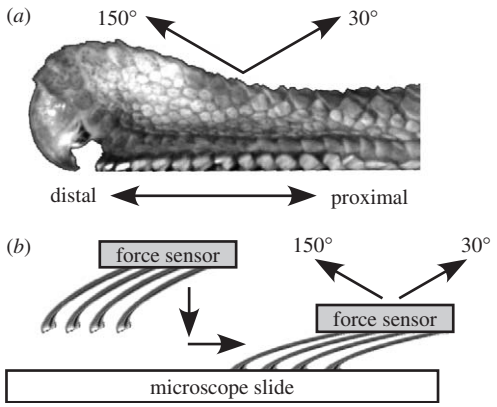

Figure 2. Geometry of isolated setal array detachment tests. (*a*) Side view of a tokay gecko toe showing the proximal (0°; towards animal) and distal (180°; away from animal) directions. (*b*) Isolated setal arrays were loaded vertically and then dragged proximally to attach. Once adhering, setal arrays were detached along a linear path of angles ranging from 30° to 150° in increments of 10°. Setal array reaction force and displacement was measured during detachment, yielding work of detachment (W_d).

microscope, we trimmed excess lamella from isolated arrays, mounted them to scanning electron microscope stubs using Loctite 410 (Henkel Co., CT) and allowed them to set overnight. To ensure no wicking of glue occurred in setal shafts, we visually inspected samples using a DFK 31AF03 digital Firewire camera (The Imaging Source, Charlotte, NC) with an attached Optem inspection microscope (Qioptiq, Fairport, NY) prior to mechanical testing. We captured whole setal array images and measured the setal-bearing area using LabVIEW image analysis software (National Instruments, Austin, TX).

2.1. Testing apparatus

Stub samples were mounted to a Kistler 9328A three-axis piezoelectric force sensor (Kistler, Winterthur, Switzerland) with the aid of a specimen chuck (figure 2). The stiffness of the system was approximately 320 N mm^{-1} (Autumn *et al.* 2006*c*), with a natural frequency in excess of 3.3 kHz. A 100 mN force produces only approximately 312.5 nm displacement, so we considered the system effectively rigid. The force sensor and sample mounted horizontally to a stainless steel 'tombstone' above a Newport RP Reliance breadboard table (Newport, Irvine, CA). Testing substrates mounted to a custom two-axis positioning system adjacent to the force sensor, composed of two Aerotech ANT-50L (Aerotech, Pittsburgh, PA) linear actuators providing nanoscale motion control over 50 mm of travel. Two Newport goniometers, GON65L and TR120BL, enabled coplanar alignment of sample stub and test substrate. We sampled force and motion data at 1 kHz. Force and displacement resolutions were approximately 2.67 mN and 10 nm, respectively. A custom LabVIEW (National Instruments, Austin, TX) program controlled test parameters and data acquisition. We used glass microscope slides (Erie Scientific, Portsmouth, NH) as test substrates. New slides soaked in a bath of 2 M NaOH (Ted Pella, Redding, CA) for 10 min prior to testing to ensure that the surface was clean and uncontaminated. We rinsed slides in DI water and wiped dry with Kimwipes (Kimberly Clark, Neenah, WI) three times before mounting.

2.2. Detachment measurements

Setal array detachment tests were displacement based. A position-controlled microscope slide engaged mounted samples and then detached along the selected detachment path at a retraction angle θ. Retraction angles are defined using 0° as proximal, 90° as vertical and 180° as distal. Through variation of θ, the amount of proximal ($x(\theta)>0$) or distal ($x(\theta)<0$) shear during detachment from a set vertical preload displacement (d) is given by the equation

$$x(\theta) = \frac{d}{\tan(\theta)}. \tag{2.1}$$

Retraction angles (θ) varied from 30° to 150° in increments of 10° with each angle tested five times in random order. We chose the range of retraction angles to be symmetric about the vertical axis (90°), and constrained between angles that allowed for investigation of a large range of proximal and distal shear. Adhesion in setal arrays requires a vertical preload followed by a proximal shear to engage setae (Autumn *et al.* 2006*a*). A preload is a compressive normal ($\theta=270°$) displacement to a set depth, while a drag is a proximal shear ($\theta=0°$) displacement. We calibrated the preload displacement for each array by measuring the position at which point a force change of 5 mN is measured during a 10 µm displacement. This position was then the sample's zero position and all preload displacements reference from it. In the protocol $\mathrm{LDP}_{\mathrm{avg}}$ (LDP, load–drag–pull), we preloaded samples to the average normal 'working depth' of a typical setal array, 35 µm, and then dragged 500 µm ($N=10$ samples$\times5$ trials$\times13$ angles$=650$). $\mathrm{LDP}_{\mathrm{avg}}$ trials produced adhesive forces prior to detachment typical of previous measurements (Autumn *et al.* 2006*c*). Detachment from 35 µm between $30°<\theta<150°$ resulted in shear displacements between $60.62\ \mu\mathrm{m}<x(\theta)<-60.62\ \mu\mathrm{m}$ as given by equation (2.1).

We were able to control the amount of adhesion in setal arrays before detaching by increasing preload depths in 1 µm increments from the zero position. We determined the preload depth at which adhesion was maximal by monitoring the relative increase or decrease in adhesion during each incremental preload. In the $\mathrm{LDP}_{\mathrm{max}}$ protocol, we preloaded additional samples to the depth that maximized adhesion force in each sample ($N=7$ samples$\times5$ trials$\times13$ angles$=455$). In $\mathrm{LDP}_{\mathrm{max}}$ trials, we dragged 100 µm prior to detachment.

Detachment velocity for all tests was 50 µm s^{-1} along the detachment path until arrays completely separated from the slide, yielding a 1.43 Hz unload cycle. To calculate array stiffness and discard any arrays damaged during the experiments, we conducted purely normal load–unload or load–pull tests at the beginning and end of each set of trials for each sample (Autumn *et al.* 2006*c*).

2.3. Calculations

A custom spline filtering algorithm in LabVIEW 8 (National Instruments, Austin, TX) compensated for force sensor drift, and a third-order Butterworth FFT algorithm set at 30 Hz in DIADem (National Instruments, Austin, TX) removed high-frequency noise. To calculate the force and energy requirements during detachment, we evaluated the force–displacement measurements: the negative force–displacement integral of the setal array unloading curve yielded the detachment energy (work required to remove the adhering sample: W_{d}) as a function of detachment retraction angle. We calculated the shear elastic coefficients for individual setae by determining a sample's total shear stiffness during the loading cycle, and then scaling by setal density ($k=(\Delta\sigma/\Delta x)\cdot(1\ \mathrm{mm}^2/14\,400\ \mathrm{seta})$). Average stress ($\sigma$) is the time integral of the force vector magnitude during unloading, normalized to both the setal area (A) and duration (T) of unloading ($\sigma=(1/(T\cdot A))\int_0^T F_{\mathrm{total}}\,\mathrm{d}t$). Results are means$\pm$s.e.m. unless otherwise noted.

3. RESULTS

Isolated tokay gecko (*G. gecko*) setal arrays exhibited frictional adhesion forces and normal effective stiffness values consistent with previous setal array measurements (Autumn *et al.* 2006*a*,*c*). Setal arrays averaged $0.93\pm0.12\ \mathrm{mm}^2$ in area, and contained approximately $13\,392\pm1728$ setae, assuming $14\,400\ \mathrm{setae\ mm}^{-2}$ (Schleich & Kästle 1986). Setal arrays preloaded to 35 μm depth and dragged ($\mathrm{LDP}_{\mathrm{avg}}$, $N=10$ arrays, 650 trials) had average proximal friction stresses of 111 ± 19.8 kPa (104 ± 30 mN) and adhesion stresses of -30 ± 6.7 kPa (-28 ± 8 mN). Arrays preloaded and dragged at individual maximum adhesive depths ($\mathrm{LDP}_{\mathrm{max}}$, $N=7$ arrays, 455 trials) had average friction stresses of 184 ± 23 kPa (171 ± 18 mN) and adhesion stresses of -48 ± 7 kPa (-45 ± 6 mN). Setal array effective elastic modulus (E_{eff}) in the normal axis averaged 117 ± 15.6 kPa with an $8\pm4\%$ decrease between initial and final detachment tests.

3.1. Detachment stress

The largest average detachment stresses (σ) for both loading conditions occurred during 30° detachment (figure 3). Adhering setal arrays exhibited large and relatively consistent σ for $\theta<110°$, at which point σ began decreasing reaching a minimum at $\theta=130°$. Maximum σ was 53 ± 7.6 kPa for strongly attached arrays ($\mathrm{LDP}_{\mathrm{max}}$ protocol) and 35 ± 9.2 kPa for arrays loaded to a 35 μm preload depth ($\mathrm{LDP}_{\mathrm{avg}}$ protocol). Minimum σ was 15 ± 1.5 kPa for $\mathrm{LDP}_{\mathrm{max}}$ trials and 12 ± 2.5 kPa for $\mathrm{LDP}_{\mathrm{avg}}$ trials.

3.2. Energy dissipation in the gecko adhesive

W_{d} varied similarly as a function of detachment angle (θ) regardless of loading method. W_{d} was maximal at the lowest retraction angle ($\theta=30°$), decreasing as θ increased. W_{d} was negative above $\theta=110°$. Maximum W_{d} was $5.0\pm0.86\ \mathrm{J\ m}^{-2}$ for maximum adhering arrays ($\mathrm{LDP}_{\mathrm{max}}$) and $3.0\pm0.81\ \mathrm{J\ m}^{-2}$ for average adhering arrays ($\mathrm{LDP}_{\mathrm{avg}}$). Negative W_{d} signifies that energy was returned upon setal array detachment, instead of being dissipated. Minimum W_{d} occurred when detaching the gecko adhesive at $\theta=130°$ signifying greatest energy return at this angle. Minimum W_{d} was $-0.8\pm0.12\ \mathrm{J\ m}^{-2}$ for maximum adhering arrays and $-0.55\pm0.09\ \mathrm{J\ m}^{-2}$ for average adhering arrays.

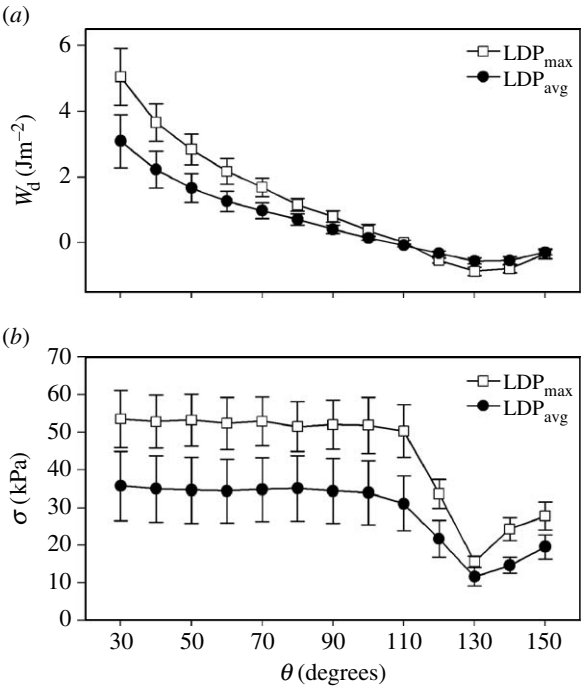

Figure 3. The mechanics of detaching isolated tokay gecko setal arrays along a path of angle θ from depths producing maximum ($\mathrm{LDP}_{\mathrm{max}}$) and average ($\mathrm{LDP}_{\mathrm{avg}}$) adhesion. $\theta=0°$ is proximal shearing, $\theta=90°$ is vertical detachment, and $\theta=180°$ is distal shearing. (*a*) The detachment energy (W_{d}) for both loading conditions was maximum at $\theta=30°$ and decreased with increasing θ becoming negative at $\theta\sim110°$ and reaching a minimum at $\theta=130°$. Maximum W_{d} was $5.0\pm0.86\ \mathrm{J\ m}^{-2}$ for $\mathrm{LDP}_{\mathrm{max}}$ and $3.0\pm0.81\ \mathrm{J\ m}^{-2}$ for $\mathrm{LDP}_{\mathrm{avg}}$. Minimum W_{d} was $-0.8\pm0.12\ \mathrm{J\ m}^{-2}$ for $\mathrm{LDP}_{\mathrm{max}}$ and $-0.55\pm0.09\ \mathrm{J\ m}^{-2}$ for $\mathrm{LDP}_{\mathrm{avg}}$. (*b*) The average detachment stress (σ) had identical extrema as W_{d} for both loading conditions. However, σ stayed relatively constant until $\theta\sim110°$, whereas W_{d} decreased steadily. Maximum σ was 53 ± 7.6 kPa for $\mathrm{LDP}_{\mathrm{max}}$ and 35 ± 9.2 kPa for $\mathrm{LDP}_{\mathrm{avg}}$. Minimum σ was 15 ± 1.5 kPa for $\mathrm{LDP}_{\mathrm{max}}$ arrays and 12 ± 2.5 kPa for $\mathrm{LDP}_{\mathrm{avg}}$.

3.3. Control of W_{d} during engagement

Attachment of setae for both $\mathrm{LDP}_{\mathrm{max}}$ and $\mathrm{LDP}_{\mathrm{avg}}$ testing methods occurred within approximately the first 10 μm of dragging, as setae elongated elastically (figure 4). Further dragging of setal arrays resulted in a change in friction of approximately 10% (figure 4), indicating that the forces present at detachment are largely unaffected by drag length. Setae generated most of the shear stress present at detachment within the first 20 μm (figure 4). Maximally adhering samples had

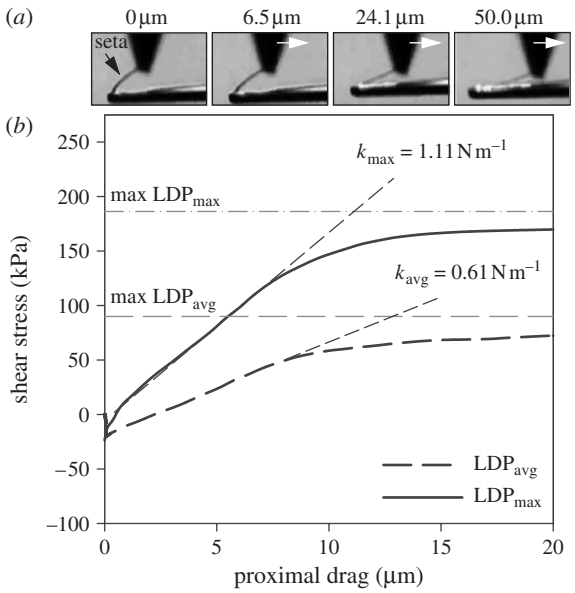

Figure 4. After a vertical preload, a proximal drag is required to engage setae in adhesion. (*a*) In a separate experiment, a single seta was observed during loading to measure the kinematics of attachment. The amount of proximal drag distance is noted for each frame showing that after approximately 20 µm the seta is fully straightened. Subsequent dragging of the seta resulted in sliding while shaft tension was maintained. (*b*) Average friction stresses measured during setal array attachment are shown for both loading methods as a function of engagement drag distance, illustrating that setae rapidly approach maximum stress during the first approximately 20 µm. The initial constant slopes indicate elastic loading for the first approximately 10 µm with setal elastic coefficients of $k_{max}=1.11$ N m^{-1} for LDP$_{max}$ and $k_{avg}=0.61$ N m^{-1} for LDP$_{avg}$. After the initial elastic loading, setal stresses began to level off as the seta straightens and tip sliding eventually occurs. Within 20 µm of dragging friction stresses are very near the stresses present at detachment.

a shear setal elastic coefficient of 1.11 N m^{-1} per seta, and average adhering arrays had a shear setal elastic coefficient of 0.605 N m^{-1} per seta. The vertical bending (transverse) stiffness of setae measured previously was 0.095 N m^{-1} per seta (Autumn *et al.* 2006*c*), indicating an approximate 10 : 1 ratio of shear setal stiffness versus vertical setal stiffness in an array.

Detachment energy (W_d) of setal arrays depended upon the engagement condition. Strongly attached setal arrays (LDP$_{max}$) required the most energy to detach at low angles, yet also returned the most energy while detaching at high angles. Arrays loaded to an average depth (LDP$_{avg}$) required less detachment energy at low angles and returned less energy detaching at high angles. Maximum W_d between loading conditions ranged from 5.0 ± 0.86 J m^{-2} (LDP$_{max}$, $\theta=30°$) to 3.0 ± 0.81 J m^{-2} (LDP$_{avg}$, $\theta=30°$) representing a 2 J m^{-2} difference in adhesive toughness controlled by engagement. Controlling the engagement of setae via preload depth affected the adhesive's toughness, but did not alter the minimum energy of detachment. W_d was minimal at $\theta=130°$ for both LDP$_{max}$ and LDP$_{avg}$ protocols and varied only by 0.25 J m^{-2} between loading conditions.

4. DISCUSSION

Gecko setae are a unique directional adhesive. Frictionally coupled adhesion forces occur when the gecko pulls its adhesive proximally (towards the animal). Pushing distally causes setae to compress, not adhere (Autumn *et al.* 2006*a*). Setae detach when the shaft angle (Autumn *et al.* 2000), or resultant force vector angle (Autumn *et al.* 2006*a*) exceeds $\alpha^*=30°$. In this study, we varied the ratio of normal to shear displacement as we separated setal arrays from the substrate to yield a linear detachment path of angle θ. We found that θ determined the amount of energy (W_d) dissipated by setae prior to reaching their critical angle of detachment. Our most proximal detachment trajectory ($\theta=30°$) resulted in the largest energy dissipation during detachment. Adhering setal arrays required approximately two orders of magnitude more W_d to remove than the thermodynamic vdW bond energy γ. Energy dissipation decreased as the detachment trajectory moved from proximal to distal. At 110°, W_d became negative, indicating that for certain trajectories energy can be returned when gecko setae detach.

Both conventional PSAs and setae adhere primarily through vdW forces and are capable of repeatable attachment under light pressure. PSAs are soft viscoelastic materials (Pocius 2002) with Young's modulus below 100 kPa at 1 Hz (Dahlquist 1969). Setae are composed of rigid beams with material elastic modulus of 1.4 GPa (Peattie *et al.* 2007) but through fibrillation the gecko adhesive's effective modulus of 100 kPa (at approx. 1 Hz) is close to that of PSAs (Autumn *et al.* 2006*c*). The maximum W_d of gecko setae is comparable to typical energies for PSAs with W_d around 2–3 orders of magnitude larger than γ (Kinloch 1987; Newby & Chaudhury 1998). However, even though setae and PSA have similar maximal W_d, we found that the mechanisms of energy dissipation in setae and PSA differ.

4.1. Elastic energy

The question of how an elastic fibrillar adhesive may dissipate energy has been approached before. Theoretically, elastic loading of fibrils during detachment can cause energy loss as fibrils eliminate local energy transfer (Jagota & Bennison 2002). Elastic potential is given by $W_{elastic}=(F^2/2k)$, where F is the pull-off force and k is the spring constant. If $W_{elastic}$ largely determines W_d, then W_d should be proportional to the elastic potential, and therefore the stress: $W_d \propto \sigma^2$. In contrast, for energy-dissipating detachment paths ($\theta<110°$), σ remained largely consistent while W_d varied greatly, suggesting absence of the stress–energy relationship and that elastic loading during detachment does not occur in adhering setal arrays.

Unloaded setae are curved and have increased axial stiffness when straightened in tension. A seta with length 110 µm, radius 2.1 µm and Young's modulus of 1.4 GPa has a curved axial stiffness of

$$k_{curved} \approx C\frac{ER^4}{L^3} \approx 0.20 \text{ N m}^{-1}. \qquad (4.1)$$

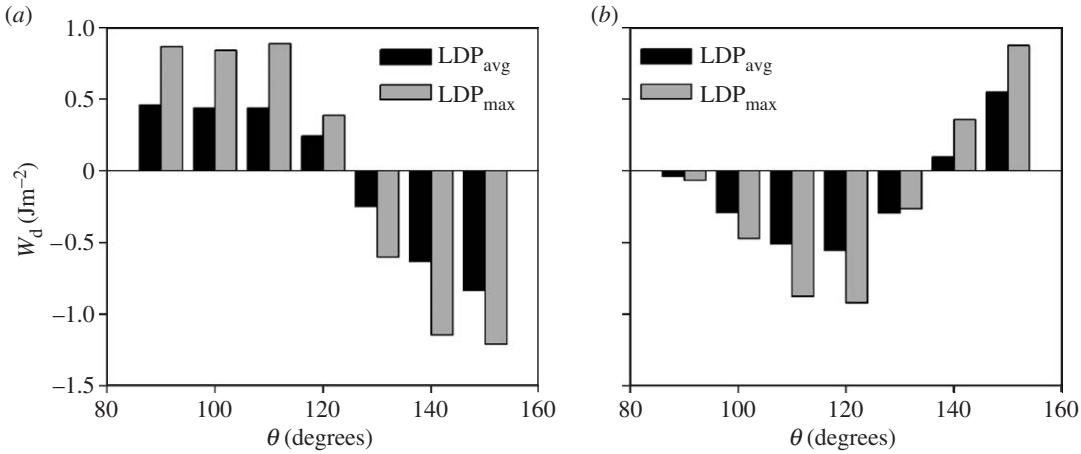

Figure 5. Detachment energy (W_d) components for distal angles ($\theta > 90°$) illustrate the elastic energy return during engagement. (*a*) Normal W_d shows that setae adhere ($W_d > 0$) up to $\theta = 120°$, after which energy is returned for greater θ. As the detachment angle becomes increasingly distal, setal tension relaxes earlier along the detachment trajectory allowing for large normal energy return during detachment. (*b*) Shear W_d becomes negative as soon as the displacement becomes distal ($\theta > 90°$), indicating that shaft tension is being relaxed elastically. Detachment at angles above 120° relaxes shafts and then begins to compress them axially resulting in an increasing W_d.

(for a constant of curvature, $C \approx 10$; Persson 2003) and a straightened axial stiffness of

$$k_{\text{straight}} = \frac{\pi R^2 E}{L} = 176.3\ \text{N m}^{-1} \tag{4.2}$$

(Sitti & Fearing 2003). This large increase in axial stiffness ($(k_{\text{curved}}/k_{\text{straight}}) \propto 10^{-3}$) suggests that axial elastic loading of setae can occur only until shafts are pulled straight. Our results suggest that setae store energy elastically only during their attachment phase and not during further loading. This is consistent with prior studies showing that setal adhesion requires a vertical preload followed by a proximal drag to adhere (Autumn *et al.* 2000). Setae generated most of their frictional adhesion forces within the first 20 µm of dragging (figure 4). Initially, setae loaded elastically with measured shear setal spring constants of $k_{\text{avg}} = 0.61\ \text{N m}^{-1}$ and $k_{\text{max}} = 1.11\ \text{N m}^{-1}$. The measured shear elastic coefficients are well within the range of axial setal stiffness values predicted from our calculation ($0.20\ \text{N m}^{-1}$, equation (4.1)) and the $6\ \text{N m}^{-1}$ calculation of Persson (2003). Thus, it is reasonable that the stiffness we measured while pulling setae in shear corresponds to the axial stiffness of the curved setal shafts as they extended. Setal forces stabilized after approximately 10 µm of dragging, indicating that as setal stiffness increased from elongation, the tips began sliding and shaft tension equilibrated. For a setal array density of $14\,400\ \text{mm}^{-2}$ with a setal stiffness range of $k = 0.61$–$1.11\ \text{N m}^{-1}$, the energy stored during the 10 µm setal array elastic loading was

$$W_{//} = \rho \frac{1}{2} k_{\text{avg}} x^2 = 0.44\ \text{J m}^{-2}, \quad K_{\text{avg}} = 0.61\ \text{N m}^{-1}, \tag{4.3}$$

$$W_{//} = \rho \frac{1}{2} k_{\text{max}} x^2 = 0.80\ \text{J m}^{-2}, \quad K_{\text{avg}} = 1.11\ \text{N m}^{-1}. \tag{4.4}$$

Equations (4.3) and (4.4) illustrate that even if elastic loading of the curved setae occurred upon detachment, it could not account fully for the large values of W_d (up to $5\ \text{J m}^{-2}$). Thus, while elastic loading of the setae is an integral part of the gecko adhesive's attachment mechanism, it does not seem to cause energy dissipation upon detachment. However, elastic energy does play a central role in energy return for highly distal detachment paths. Equations (4.1) and (4.2) suggest that setae pulled proximally during loading straighten and become effectively inextensible (figure 4), limiting possible elastic energy dissipation. However, elastic unloading of setae did occur during detachment, causing energy to return to the system. The minimum values of W_d represent the maximum amount of energy returned during detachment at path angle θ. Previous tests on polytetrafluoroethylene showed that non-adhering setae return nearly all elastically stored energy during unloading (Autumn *et al.* 2006*c*). Setal attachment requires normal and proximal/shear loading, which account for the net elastic energy that is returned when detaching along paths of $\theta > 110°$. Equations (4.3) and (4.4) predict that $0.44\ \text{J m}^{-2}$ (LDP_{avg}) and $0.80\ \text{J m}^{-2}$ (LDP_{max}) of shear elastic energy was stored during attachment. This is similar to the maximum energy return in the shear direction of $-0.56 \pm 0.1\ \text{J m}^{-2}$ (LDP_{avg}) and $-0.92 \pm 0.08\ \text{J m}^{-2}$ (LDP_{max}) both at 120° (figure 5). Vertical loading of the gecko adhesive to a depth of 35 µm with average effective elastic modulus 117 kPa and approximate height of 70 µm (Autumn *et al.* 2006*c*), results in $W_{\perp} = (E_{\text{eff}}(\Delta H)^2/2H_0) = 0.875\ \text{J m}^{-2}$ of normal elastic energy. The maximum energy return in the normal direction for LDP_{avg} was $-0.84 \pm 0.1\ \text{J m}^{-2}$ at 150°, indicating that approximately 96% of normal elastic energy may be returned at higher angles.

4.2. Frictional detachment

Once setae are loaded fully by the load and drag steps, additional shear causes setal tips to slide along the substrate (figure 4). Consistent friction and adhesion forces for drags above approximately 20 µm (figure 4)

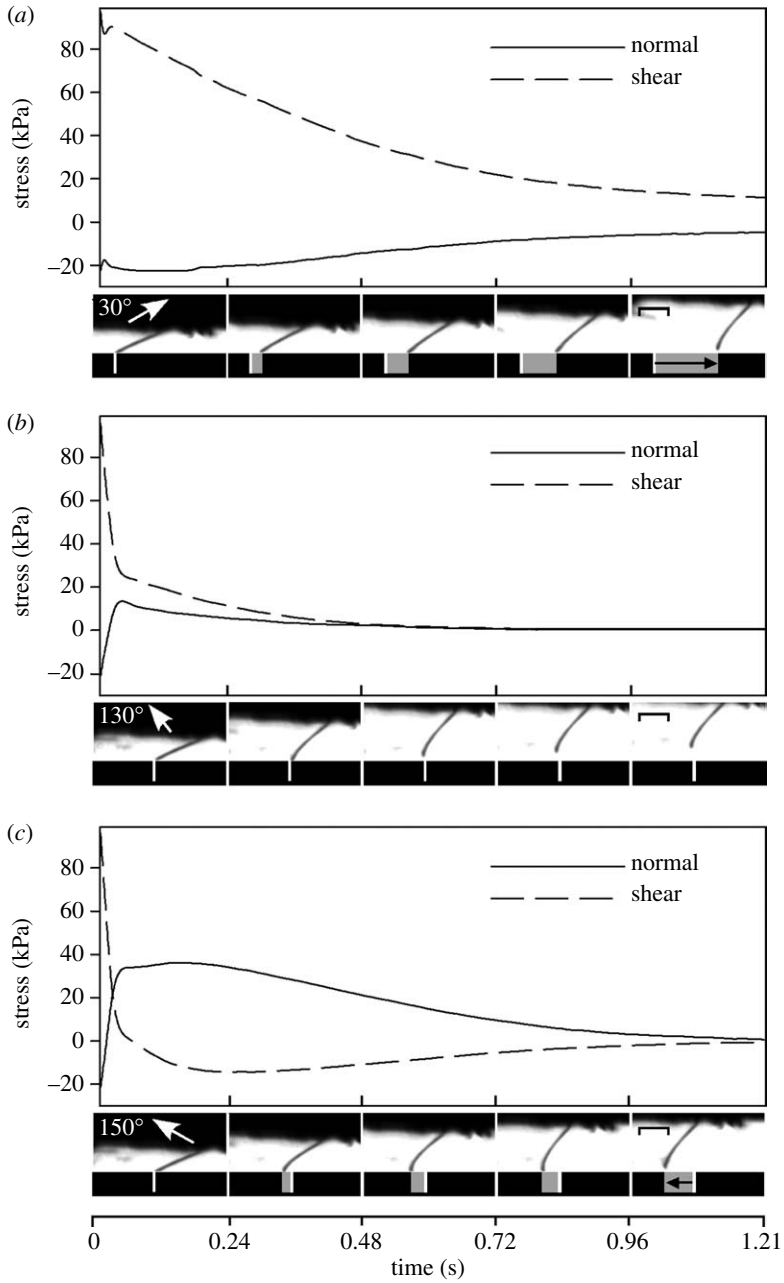

Figure 6. Average unloading friction and adhesion curves from setal array detachment tests (LDP_{avg}) are shown for three detachment angles. For each detachment angle, a sequence of still images from a video of a single seta illustrates the kinematics of detachment at that angle. Positive shear force indicates that setae are pulled in tension, and a negative normal force indicates that setae are adhering. The white line in the single seta image sequences indicates the initial setal tip position prior to detachment, and the grey bar shows the total distance of tip sliding. The last frame of each sequence has a 50 μm scale bar in the upper left corner. Left tip displacement is distal and right tip displacement is proximal. (*a*) Detaching along a linear path oriented at 30° causes shafts to remain in tension during detachment. The shear force slowly decreases during the largely proximal detachment path until removed from the surface. The setae adhered during the whole detachment motion requiring a large energy input necessary to detach. The single seta images show that the tip slid approximately 30–50 μm prior to detachment. (*b*) Detachment along a 130° linear path resulted in a rapid decrease of both shear and normal force signifying that shaft tension was released rapidly. The single seta images show no tip displacement during the entire unloading cycle. This suggests that 130° is the optimum detachment angle because it allows elastic shaft energy to return without dissipating any energy frictionally. (*c*) A linear detachment path oriented at 150° resulted in a rapid decrease of shear force and normal force. However instead of remaining small, the shear and normal forces became substantially large in the opposite direction indicating that the setae was compressing during detachment. The image sequence shows that, at such a high detachment angle, the shaft is compressing axially and sliding during detachment, which resulted in energy dissipation and inefficient detachment.

show that sliding maintains constant shaft tension. Therefore, detaching setae already in tension causes setal tip sliding and results in frictional energy dissipation. In figure 6, tip sliding is shown for a 30° linear detachment path where substantial sliding between the spatula and substrate occurs as the setae detach. The average sliding friction stress for a setal array was 111 kPa: for just 10 μm of tip sliding during detachment, $W = \sigma \cdot d = 1.1\ \mathrm{J\ m^{-2}}$ of energy could be dissipated.

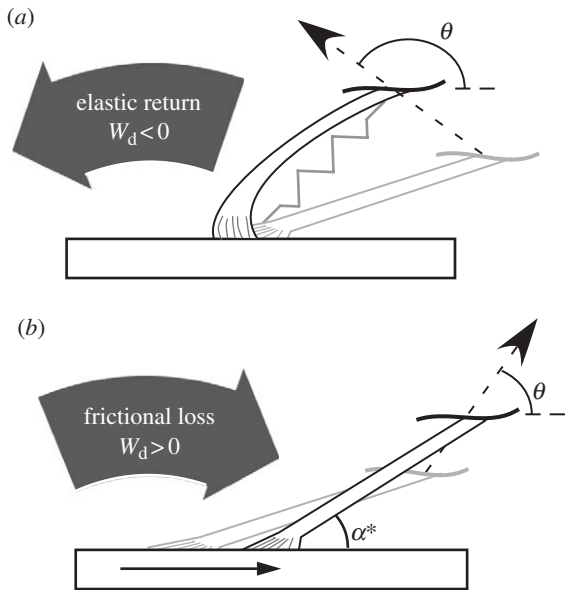

Figure 7. Frictional ($W_d>0$) and spring-loaded ($W_d<0$) detachment mechanics for an individual seta detaching over a retraction angle θ. Grey arrows illustrate the net energy input (towards the system) and output (away form the system) that occur. (*a*) During detachment along a 130° linear path, the setal tip remains stationary while the shaft unloads elastically, resulting in spontaneous debonding ($W_d<0$). (*b*) A largely proximal linear detachment path causes setae to remain in tension, inhibiting elastic energy return to the system. The setal tip slides along the substrate during separation until the setal shaft angle reaches the critical angle of detachment $\alpha^*=26$–$30°$, at which point debonding occurs. The setal tip sliding that occurs prior to debonding results in frictional energy loss during detachment and thus a large W_d.

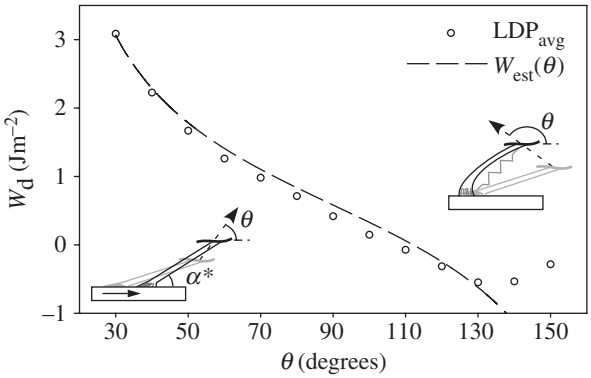

Figure 8. Frictional tip sliding results in detachment energy dissipation (W_d) that varies as a function of θ. Modelling a seta in tension as a rigid rotatable beam W_d can be approximated as $W_{est}(\theta)=F\cdot s(\theta)$ from the geometric tip displacement $s(\theta)$ of the detaching beam. A seta 110 μm in length is loaded 35 μm from its original height of 70 μm making an initial 18° shaft-substrate angle that increases until detachment occurs at $\alpha=26°$. Assuming an average setal stress of 161 kPa produces the fit for W_d. The illustration inset in the bottom left corner highlights the frictional sliding of the setal tips during detachment ($\theta<110°$). The illustration inset on the right side shows how negative energy results from the spring-loaded setae unloading during high angle detachment ($\theta>110°$).

Viscoelastic energy loss is the dominant mechanism for tenacious adhesion of PSAs. Energy dissipation in PSA detachment occurs as a result of internal friction during the deformation of the PSA medium (Bhushan 2002; Creton 2003). In contrast, energy dissipation in the gecko adhesive occurs through external friction at the seta–substrate interface. Thus, the gecko adhesive possesses the 'viscous' energy-dissipating properties of PSAs, yet is able to maintain its structure and adhesive capability over many loading/unloading cycles without the material degradation associated with plastic deformation. Frictional energy dissipation has also been shown to occur in the asymmetric detachment of PSA interfaces, where friction accounts for up to 75% of the total fracture energy measured (Newby & Chaudhury 1998). Viscous shear deformation of PSAs is analogous to the ability of setae to absorb large amounts of energy as they slide along the substrate during detachment. However, in addition to dissipating frictional energy during detachment, setal curvature enables efficient spring loaded detachment (figure 7) unattainable in PSAs.

Frictional energy dissipation can be modelled by assuming that a setal shaft in tension acts as an inextensible beam free to rotate. Vertically preloading an approximately 70 μm tall setal array to half its height ($d=35$ μm; Autumn *et al.* 2006*c*) will cause the shaft angle of a $L=110$ μm long seta to rotate to an angle of

$$\alpha_0=\sin^{-1}\left(\frac{H-d}{L}\right)=18^\circ. \tag{4.5}$$

The seta's initial shaft-substrate angle is α_0 and α increases during detachment as the setal base moves along a linear path of angle θ until α reaches the critical angle of detachment $\alpha^*=26$–$30°$ (Autumn *et al.* 2006*a*) at which point setae detach spontaneously. The shear tip displacement along a substrate during detachment of an inextensible seta of length L and retraction angle (θ) is

$$s(\theta)=L\left(\cos(\alpha_0)-\cos(\alpha^*)+\frac{\sin(\alpha^*)-\sin(\alpha_0)}{\tan(\theta)}\right) \tag{4.6}$$

Estimating frictional work as $W_{est}(\theta)=\sigma_{friction}\cdot s(\theta)$ where $s(\theta)$ is the tip displacement from equation (4.6), we found that a constant setal friction stress of 161 kPa could account for W_d (figure 8). This stress value is consistent with our drag friction measurement of 111 ± 19.8 kPa (Autumn 2006*b*).

Setae in tension typically slide only proximally because distal base motion results in shaft unloading. Frictional energy dissipation ($W_d>0$) occurs mostly when the tip is sliding proximally during detachment. Using equation (4.6), we calculate that proximal tip displacement of a tokay gecko seta of length 110 μm ($\alpha^*=26$–$30°$) (Autumn *et al.* 2006*a*), preloaded 35 μm ($\alpha^*=18°$, equation (4.5)) should occur only for detachment angles below 112°, at which point tip motion theoretically becomes distal ($s(\theta)<0$). Energy dissipation in the real gecko setal arrays occurred for paths below 110° almost exactly matching this 112° predicted detachment path.

4.3. Optimal detachment requires minimizing friction and maximizing elastic return

Setae in their non-adhering default state are curved (Autumn & Hansen 2006), and not yet in tension. Previously, we found that non-adhering setae act as nearly ideal springs (Autumn & Hansen 2006; Autumn *et al.* 2006*c*). In this study, detaching at increasingly higher angles resulted in relaxation earlier in the detachment trajectory and thus more normal energy is returned (figure 6). However, detaching at paths above $\theta = 120°$ also resulted in axial compression, causing an increase in shear energy returned (figures 5 and 6). At $\theta = 130°$, there is the best balance of energy return between the shear and normal components. Detaching at $\theta = 130°$ causes no tip sliding to occur during detachment and no further energy dissipation occurs (figure 6). Thus, maximum energy is returned during unloading of the setae at the optimal angle of $\theta = 130°$.

5. CONCLUSION

Gecko setae adhere strongly to nearly any surface yet detach rapidly and efficiently, unlike conventional PSAs, which are either strong and hard-to-remove or easy-to-remove but weak. For example, duct tape or double-sided tape attach strongly, but large detachment energies ($W_d \gg \gamma$) are also required to remove these adhesives. Sticky notes detach easily, yet their attachment is weak. The gecko adhesive is special in its ability to both adhere strongly (large W_d) and detach efficiently (negative W_d). The spring-loaded detachment mechanism is unique among adhesives and suggests that curved shafts capable of storing elastic energy in elongation (Federle 2006) are a key design principle enabling efficient detachment.

Setal shafts are curved in their unloaded default state (Autumn & Hansen 2006), and store elastic energy as they elongate under tension. We found that elastic energy was returned when the adhesive was detached at an angle $\theta = 130°$ (figure 6), resulting in spontaneous (energy-free) detachment. Since attached setae are in tension, a sustained proximal force is required to resist spontaneous detachment (Russell 2002). This supports the frictional adhesion model (Autumn *et al.* 2006*a*), which is based on the observation that adhesion is a linear function of the applied shear force and consistent with measurements of the forces geckos apply while climbing (Autumn *et al.* 2006*b*; and see the electronic supplementary material).

We dragged setae over a proximal distance of 100–500 μm, possibly greater than the distance live geckos drag their adhesive during climbing. However, within the first 20 μm of dragging, isolated setae developed 75–90% of maximal friction and adhesion forces, with subsequent displacement resulting in little change in force. This suggests that the conclusions of this study are likely to be valid for geckos climbing in nature. The ability of gecko setae to sustain kinetic friction and dissipate energy under negative (adhesive) loads may also confer advantages to animals recovering from falls or resisting perturbations that exceed the static capacities of the adhesive (Autumn 2006*a*).

Elastic energy storage has been proposed as a mechanism for energy dissipation in the gecko adhesive (Jagota & Bennison 2002). Our study illustrates that while elastic extension is required for setae to attach properly, elastic energy does not contribute substantially to W_d owing to the high stiffness of curved shafts once they elongate (equations (4.1) and (4.2)). Instead, as setae unbend, spatulae slide along the substrate and dissipate energy frictionally. We found that the optimum detachment path of $\theta = 130°$ for isolated tokay gecko setae resulted in no tip displacement (and thus no frictional dissipation) during detachment (figure 6). The ratio of elastic to frictional contributions to W_d will probably increase in fibrillar adhesives fabricated from materials with lower Young's moduli (Spolenak *et al.* 2005).

The energy-dissipating properties of gecko setae suggest industrial uses for synthetic gecko adhesives that are quite different from typical adhesive applications. For instance, shock absorbers and brakes are energy-dissipating systems standard on every automobile. Braking systems rely on traditional frictional mechanics by applying a large normal force to the calliper to create a frictional stopping force. However, a braking system using a synthetic gecko adhesive would not require a large normal load but instead would operate under its own adhesive force, eliminating the need for hydraulic pistons. From our measurements, a gecko brake could dissipate up to 1.8×10^5 J m^{-2} for every metre dragged. A 1000 kg automobile moving at 80 km h^{-1} would require $E = (1/2)mv^2 = 2.50 \times 10^5$ J to come to a complete stop. Stopping this automobile in 5 m would require only $A = (2.5 \times 10^5 \text{J})/((5\text{ m})(1.8 \times 10^5 \text{J m}^{-3})) = 0.28$ m^2 of gecko adhesive.

We thank Jacob Israelachvili, Tony Russell, Carmel Majidi, Anne Peattie, Jorn Cheney and Ananda Ellis. Research was supported by DARPA N66001-03-C-8045, NSF-NIRT 0304730, DCI/NGIA HM1582-05-2022 grants, Emhart Corporation and a gift from Johnson & Johnson Dupuy-Mitek Corp.

REFERENCES

Autumn, K. 2006*a* How gecko toes stick. *Am. Sci.* **94**, 124–132. (doi:10.1511/2006.2.124)

Autumn, K. 2006*b* Properties, principles, and parameters of the gecko adhesive system. In *Biological adhesives* (eds A. Smith & J. Callow), pp. 225–255. Berlin, Germany: Springer.

Autumn, K. & Hansen, W. 2006 Ultrahydrophobicity indicates a nonadhesive default state in gecko setae. *J. Comp. Physiol. A* **192**, 1205–1212. (doi:10.1007/s00359-006-0149-y)

Autumn, K., Liang, Y. A., Hsieh, S. T., Zesch, W., Chan, W.-P., Kenny, W. T., Fearing, R. & Full, R. J. 2000 Adhesive force of a single gecko foot-hair. *Nature* **405**, 681–685. (doi:10.1038/35015073)

Autumn, K. *et al.* 2002 Evidence for van der Waals adhesion in gecko setae. *Proc. Natl Acad. Sci. USA* **99**, 12 252–12 256. (doi:10.1073/pnas.192252799)

Autumn, K., Dittmore, A., Santos, D., Spenko, M. & Cutkosky, M. 2006*a* Frictional adhesion: a new angle on gecko attachment. *J. Exp. Biol.* **209**, 3569–3579. (doi:10.1242/jeb.02486)

Autumn, K., Hsieh, S. T., Dudek, D. M., Chen, J., Chitaphan, C. & Full, R. J. 2006*b* Dynamics of geckos running vertically. *J. Exp. Biol.* **209**, 260–272. (doi:10.1242/jeb.01980)

Autumn, K., Majidi, C., Groff, R., Dittmore, A. & Fearing, R. 2006*c* Effective elastic modulus of isolated gecko setal arrays. *J. Exp. Biol.* **209**, 3558–3568. (doi:10.1242/jeb.02469)

Bhushan, B. 2002 *Introduction to tribology*. New York, NY: Wiley.

Creton, C. 2003 Pressure-sensitive adhesives: an introductory course. *MRS Bull.* **28**, 434–439.

Creton, C. & Fabre, P. 2002 Tack. In *Adhesion science and engineering, vol. I: the mechanics of adhesion*, vol. 1 (eds D. Dillard & A. Pocius), pp. 535–576. Amsterdam, The Netherlands: Elsevier.

Dahlquist, C. A. 1969 Pressure-sensitive adhesives. In *Treatise on adhesion and adhesives*, vol. 2 (ed. R. L. Patrick), pp. 219–260. New York, NY: Dekker.

Fakley, M. 2001 Smart adhesives. *Chem. Ind.* **21**, 691–695.

Federle, W. 2006 Why are so many adhesive pads hairy? *J. Exp. Biol.* **209**, 2611–2621. (doi:10.1242/jeb.02323)

Hansen, W. & Autumn, K. 2005 Evidence for self-cleaning in gecko setae. *Proc. Natl Acad. Sci. USA* **102**, 385–389. (doi:10.1073/pnas.0408304102)

Israelachvili, J. 1992 *Intermolecular and surface forces*. New York, NY: Academic Press.

Jagota, A. & Bennison, S. 2002 Mechanics of adhesion through a fibrillar microstructure. *Int. Comp. Biol.* **42**, 1140–1145. (doi:10.1093/icb/42.6.1140)

Kinloch, A. J. 1987 *Adhesion and adhesives: science and technology*. New York, NY: Chapman and Hall.

Lake, G. & Thomas, A. 1967 The strength of highly elastic materials. *Proc. R. Soc. A* **300**, 108–119. (doi:10.1098/rspa.1967.0160)

Newby, B. M. Z. & Chaudhury, M. K. 1998 Friction in adhesion. *Langmuir* **14**, 4865–4872. (doi:10.1021/la980290l)

Peattie, A. M., Majidi, C., Corder, A. & Full, R. J. 2007 Ancestrally high elastic modulus of gecko setal β-keratin. *J. R. Soc. Interface* **4**, 1071–1076. (doi:10.1098/rsif.2007.0226)

Persson, B. N. J. 2003 On the mechanism of adhesion in biological systems. *J. Chem. Phys.* **118**, 7614–7621. (doi:10.1063/1.1562192)

Pocius, A. V. 2002 *Adhesion and adhesives technology: an introduction*, 2nd edn. Munich, Germany: Hanser Verlag.

Ruibal, R. & Ernst, V. 1965 The structure of the digital setae of lizards. *J. Morphol.* **117**, 271–294. (doi:10.1002/jmor.1051170302)

Russell, A. P. 1975 A contribution to the functional morphology of the foot of the tokay, *Gekko gecko* (Reptilia, Gekkonidae). *J. Zool.* **176**, 437–476.

Russell, A. P. 2002 Integrative functional morphology of the gekkotan adhesive system (Reptilia: Gekkota). *Integr. Comp. Biol.* **42**, 1154–1163. (doi:10.1093/icb/42.6.1154)

Schleich, H. H. & Kästle, W. 1986 Ultrastrukturen an Gecko-Zehen (Reptilia: Sauria: Gekkonidae). *Amphibia-Reptilia* **7**, 141–166.

Sitti, M. & Fearing, R. S. 2003 Synthetic gecko foot-hair micro/nano structures as dry adhesives. *J. Adhes. Sci. Technol.* **17**, 1055–1073. (doi:10.1163/156856103322113788)

Spolenak, R., Gorb, S. & Arzt, E. 2005 Adhesion design maps for bio-inspired attachment systems. *Acta Biomaterialia* **1**, 5–13. (doi:10.1016/j.actbio.2004.08.004)

Tian, Y., Pesika, N., Zeng, H., Rosenberg, K., Zhao, B., McGuiggan, P., Autumn, K. & Israelachvili, J. 2006 Adhesion and friction in gecko toe attachment and detachment. *Proc. Natl Acad. Sci. USA* **103**, 19 320–19 325. (doi:10.1073/pnas.0608841103)

Williams, E. E. & Peterson, J. A. 1982 Convergent and alternative designs in the digital adhesive pads of scincid lizards. *Science* **215**, 1509–1511. (doi:10.1126/science.215.4539.1509)

Zosel, A. 1985 Adhesion and tack of polymers—influence of mechanical-properties and surface tensions. *Colloid. Polym. Sci.* **263**, 541–553. (doi:10.1007/BF01421887)